λ-Repressor Oligomerization Kinetics at High Concentrations Using Fluorescence Correlation Spectroscopy in Zero-Mode Waveguides

K. T. Samiee,* M. Foquet,* L. Guo,† E. C. Cox,† and H. G. Craighead*
*School of Applied & Engineering Physics, Cornell University, Ithaca, New York 14853; and †Department of Molecular Biology, Princeton University, Princeton, New Jersey 08544

ABSTRACT Fluorescence correlation spectroscopy (FCS) has demonstrated its utility for measuring transport properties and kinetics at low fluorophore concentrations. In this article, we demonstrate that simple optical nanostructures, known as zero-mode waveguides, can be used to significantly reduce the FCS observation volume. This, in turn, allows FCS to be applied to solutions with significantly higher fluorophore concentrations. We derive an empirical FCS model accounting for one-dimensional diffusion in a finite tube with a simple exponential observation profile. This technique is used to measure the oligomerization of the bacteriophage λ repressor protein at micromolar concentrations. The results agree with previous studies utilizing conventional techniques. Additionally, we demonstrate that the zero-mode waveguides can be used to assay biological activity by measuring changes in diffusion constant as a result of ligand binding.

INTRODUCTION

A complete understanding of key metabolic pathways and genetic control systems relies on a detailed understanding of the interactions between the biochemical constituents. Studies of these interactions frequently require extensive cloning and possibly labeling one or more components of the system with radioisotopes. Mobility shift assays and chromatography can then be used to determine interaction kinetics. Although these techniques have been successful, the amount of material, preparation time, and experimental complexity can be high.

Since its introduction several decades ago, florescence correlation spectroscopy (FCS) has been used extensively to study biological and chemical reactions both in vitro and in vivo (Cluzel et al., 2000; Webb, 2001). This technique has allowed the study of diffusive properties of fluorescent probes in systems ranging from polymer networks to subcellular compartments (Gennerich and Schild, 2000; McCain et al., 2004). FCS requires considerably less reagent than chromatography or mobility shift assays and relies on fluorescent tagging, thus alleviating the need for labeling with radioisotopes. Recent studies include characterization of protein folding dynamics as well as investigations into the intracellular mobility of macromolecules (Rischel et al., 2003; Schmiedeberg et al., 2004). FCS studies rely on fluorophore concentrations that yield around a single fluorescent molecule in the observation volume at a time. With typical diffraction limited systems restricted to femtoliter or larger observation volumes, fluorophore concentrations are limited to the pico- to nanomolar range.

Studies of systems that involve ligand binding or chemical change frequently require micromolar or higher reagent concentrations. For FCS to be applied to these systems, such as dimerization reactions that occur at high concentrations, it is necessary to reduce the observation volume. Attempts to work at higher concentrations include the use of near-field scanning optical microscopy and total internal reflection to produce an evanescent illumination profile (de Lange et al., 2001). These techniques can effectively reduce the observation volume by an order of magnitude or more, and both have been used to study single molecules (Betzig and Chichester, 1993; Mashanov et al., 2003). Nanofabricated channels have also been used as a means of confining fluorescent probes and have the added benefit of increasing the rate of single molecule observations (Foquet et al., 2004). Each of these techniques has increased the working concentration. However, none has achieved the three order of magnitude decrease in observation volume required to apply FCS to a multitude of systems that function at higher concentrations.

Zero-mode waveguides provide an excellent means of volume confinement for single molecule studies at high concentrations (Levene et al., 2003). The waveguides have been implemented as small holes in a thin aluminum film on a fused silica substrate. Fluorescence is induced by a laser coupled to the waveguide via a confocal microscope in epi-illumination mode. The diameter of the metal waveguide, generally <50 nm, prevents any guided modes and hence produces a radially confined evanescent field with a total volume on the order of 10^{-21} l (Fig. 1). This observation volume makes concentrations higher than 10 μM accessible to FCS experiments and allows one to apply this simple, versatile technique to previously inaccessible biosystems (Fig. 2).

Here we report on the use of zero-mode waveguides to study the oligomerization of the bacteriophage λ repressor

Submitted September 14, 2004, and accepted for publication November 18, 2004.

Address reprint requests to Harold Craighead, C. W. Lake Jr. Professor of Engineering, Applied Physics, 205 Clark Hall, Cornell University, Ithaca, NY 14853. Tel.: 607-255-8707; E-mail: hgc1@cornell.edu.

0006-3495/05/03/2145/09 $2.00

doi: 10.1529/biophysj.104.052795

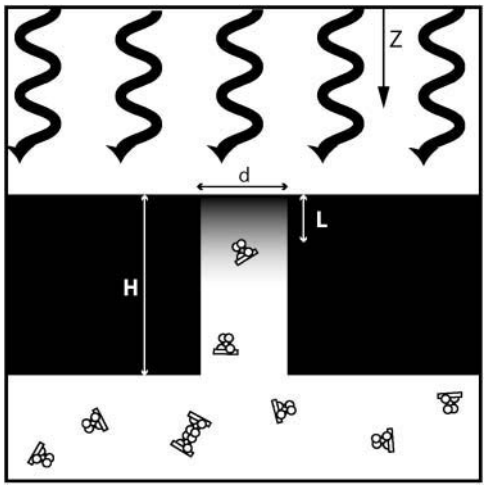

FIGURE 1 Zero-mode waveguides are 50 nm in diameter by 100 nm deep holes in an aluminum film deposited on a fused silica substrate. They are excited by confocal epi-illumination which produces an atto- to zeptoliter illumination volume at the excited end. Fluorescence generated by the molecules in the observation volume is collected back through the end of the waveguide by a microscope objective. The incident, circularly polarized light, propagates in the z direction.

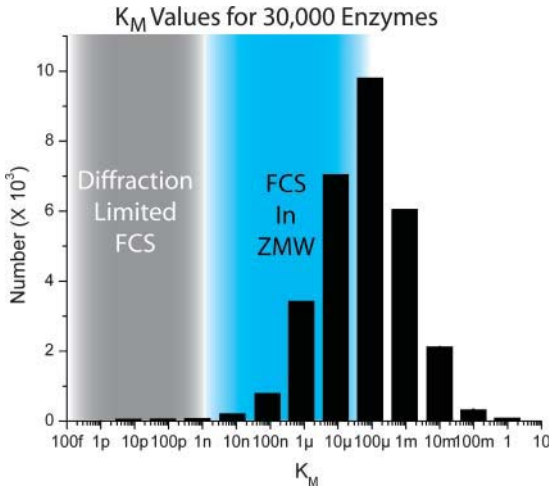

FIGURE 2 Histogram of K_M values for 30,000 enzymes taken from the Brenda Database (www.brenda.uni-koeln.de). The effective concentration ranges for diffraction limited and zero-mode waveguide FCS are shown in blue and red, respectively. Kinetics for the vast majority of enzymes are out of reach for diffraction limited FCS. FCS is not yet a viable tool above the 100 μM regime.

protein, CI. This protein controls the fate of infecting bacteriophage particles. If the CI concentration in the cell is not high enough, the viral genome will replicate, produce more bacteriophage, and lyse the host cell (the lytic cycle). The viral genome can also integrate into the *Escherichia coli* host genome, where it is switched off, lying dormant for an indefinite period (the lysogenic state; Ptashne, 1992). How this is accomplished remains an active area of research, but in broad outline, CI can either activate or suppress its own transcription. At low concentrations, the bacteriophage genes escape CI regulation because the CI-specific operator sites are underoccupied. At higher concentrations, CI forms tetramers, which interact with two sets of operator sequences 2.4 kb apart, and in this state a weak promoter, P_{RM}, is activated, leading to additional CI synthesis (Fig. 3, *A* and *B*). At yet higher intracellular concentrations, a third tetramer occupies the remaining weak operator sites O_R3 and O_L3 preventing further CI synthesis. Thus CI regulation is a subtle balance between operator affinity and location and the oligomeric state of CI (Dodd et al., 2001).

The kinetics of CI oligomerization have been extensively studied by Ackers (Pray et al., 1998); and although not all forward and reverse rates at each step on the path from monomer to octamer are known, many are (Fig. 3 *C*). Previous work indicates that dimers become the dominant species at 100 nM total CI concentration. The small tetramer

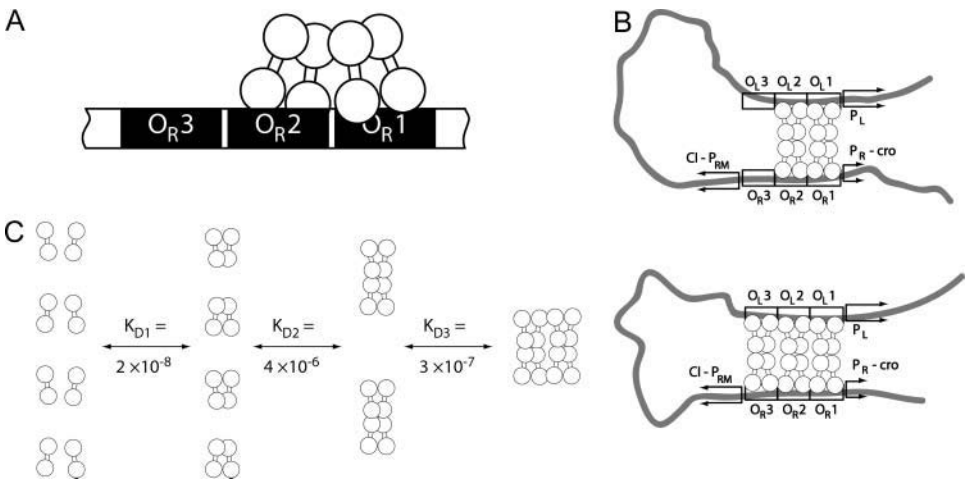

FIGURE 3 (*A*) Two CI dimers cooperatively bound to the O_R1 and O_R2 operator sites. When bound, they prevent the transcription of genes responsible for the bacteriophage's lytic path and enhance the transcription of CI. (*B*) When the concentration of CI is high enough, the proteins bound to the right operator (O_R) octamerize with CI bound to the left operator (O_L). This induces a loop structure in the DNA that leaves P_{RM} active (*top*). The loop structure enables binding of a third CI tetramer to the O_R3 and O_L3 binding site (*bottom*). This prevents RNA polymerase from binding to P_{RM} and terminates CI production. (*C*) Oligomerization kinetics established by convention biochemical techniques.

concentration peaks above 1 μM total CI concentration but rapidly decreases as octamers become the dominant species at higher concentrations (Pray et al., 1998). The formation of CI tetramers and octamers occurs at concentrations substantially higher than a few nanomolar and, consequently, cannot be studied by traditional FCS techniques. The formation of tetramers from dimers is the rate limiting step in the octamerization at high concentration (Burz and Ackers, 1996). Zero-mode waveguides were used to find the binding constant, K_{D2}, that governs the formation of CI tetramers at micromolar CI concentrations.

THEORY AND MODELING

FCS allows the measurement of diffusion constants and reaction rates in chemically reacting systems that include a fluorescent probe (Elson and Magde, 1974). The technique relies on the observation of fluorophores, typically excited by epi-illumination, as they pass through a well-defined observation volume. Autocorrelating the fluorescence intensity signal yields a curve with a shape governed by the fundamental physical properties of the system (Elson and Magde, 1974). Quantitative values can be extracted by fitting the autocorrelation curve to a theoretical model.

The precise shape of the autocorrelation curve is closely tied to the shape of the observation volume. The observation volume is defined by both the shape and intensity of the excitation illumination and the spatial sensitivity of the detection apparatus (Hess and Webb, 2002). Examining the profile of an evanescent wave below the cutoff frequency in a metallic waveguide yields the following relationship between the illumination profile and the waveguide diameter, d (Jackson, 1999):

$$\eta = \frac{1}{2}\left[\left(\frac{1}{\lambda}\right)^2 - \left(\frac{1}{\lambda_c}\right)^2\right]^{-\frac{1}{2}} = \frac{1}{2}\left[\left(\frac{1}{\lambda}\right)^2 - \left(\frac{1}{1.7d}\right)^2\right]^{-\frac{1}{2}}, \quad (1)$$

where λ is the wavelength of excitation illumination and $\lambda_c = 1.7d$ is the waveguide's cutoff wavelength. The transverse field intensity is assumed to be uniform so that the intensity profile is given by $I(x,y,z) = e^{-z/\eta}$. If the fluorophore's coupling efficiency and quantum efficiency are assumed to be proportional to the intensity profile, then the zero-mode waveguide's observation profile can be approximated by an exponential decay in one dimension, $S(z) = e^{-z/L} = e^{-3z/\eta}$, where L sets the length scale for the decay. This yields an observation volume given by

$$V_{Obs} = \frac{\pi d^2}{4}\frac{(\int S(z)dz)^2}{\int S^2(z)dz} = \frac{\pi d^2 L}{8} = 1.56\pi\frac{L^3\lambda^2}{(\lambda^2 - 36L^2)}, \quad (2)$$

where d is the diameter of the zero-mode waveguide. For a 50 nm hole, L is ~14 nm and V_{Obs} is ~14 zl corresponding to a working concentration of ~100 μM.

Because the transverse illumination is essentially uniform in small waveguides, diffusion of fluorescent species in the zero-mode waveguides is expected to appear one dimensional. Consequently, the autocorrelation curve is given by

$$G(\tau) = \int \mathrm{dzdz'}S(\mathrm{z})S(\mathrm{z'})\varphi(\mathrm{z},\mathrm{z'},\tau) = \int \mathrm{d}\upsilon\,\hat{S}^2(\upsilon)\,\hat{\varphi}(\upsilon,\tau), \quad (3)$$

where ϕ is the concentration correlation function, a hat denotes the Fourier transform, and $S(z)$ is the observation profile approximated by $e^{-z/L}$ (Elson and Magde, 1974). Taking the Fourier transform of the observation profile and substituting the solution of the diffusion equation for the concentration correlation function yields

$$G(\tau) \propto \int \frac{\mathrm{L}^2 \mathrm{e}^{-\upsilon^2\tau_\mathrm{D}}\mathrm{d}\upsilon}{(1+\mathrm{L}^2\upsilon^2)^2}. \quad (4)$$

This equation has an analytical solution; however, it does not properly describe a zero-mode waveguide of finite length. Fluorophores diffusing in and out of zero-mode waveguides are only reasonably approximated by one-dimensional diffusion. Once a fluorescent diffuser leaves the waveguide, the probability of returning to the focal volume becomes exceedingly remote as the diffuser experiences three-dimensional diffusion in the bulk solution outside the waveguide. This results in a depressed return probability at long times, and consequently the long time tail of the autocorrelation curve is depressed compared to a system experiencing true one-dimensional diffusion. To correct the model, Fourier components of the autocorrelation function with wavelengths exceeding the height, H, of the waveguide are excluded from the final integration (Levene et al., 2003). No analytical solution was found for the resulting integral, taken from $1/H$ to infinity, which complicates the fitting procedure.

An approximation yields a suitable fitting function. Let R be the ratio of the observation volume decay constant to the height of the waveguide, L/H, and let the diffusion time, τ_d, be defined as L^2/D. A change of variables yields

$$G(\tau) \propto \int_R^\infty \frac{\mathrm{e}^{-\upsilon^2\frac{\tau}{\tau_\mathrm{d}}}\mathrm{d}\upsilon}{(1+\upsilon^2)^2} = \int_0^\infty \frac{\mathrm{e}^{-\upsilon^2\frac{\tau}{\tau_\mathrm{d}}}\mathrm{d}\upsilon}{(1+\upsilon^2)^2} - \int_0^R \frac{\mathrm{e}^{-\upsilon^2\frac{\tau}{\tau_\mathrm{d}}}\mathrm{d}\upsilon}{(1+\upsilon^2)^2}. \quad (5)$$

This is simply the analytical solution for 1D diffusion minus a correction factor. The denominator of the correction factor is bounded by 1 and $(1 + R^2)^2$. The correction term can be bounded from above by a scaled error function

$$\sqrt{\frac{\tau_\mathrm{d}}{\tau}}erf(R) = \int_0^R \mathrm{e}^{-\upsilon^2\frac{\tau}{\tau_\mathrm{d}}}\,\mathrm{d}\upsilon \geq \int_0^R \frac{\mathrm{e}^{-\upsilon^2\frac{\tau}{\tau_\mathrm{d}}}\mathrm{d}\upsilon}{(1+\upsilon^2)^2} \quad (6)$$

and below by a scaled error function:

$$\int_0^R \frac{\mathrm{e}^{-\upsilon^2\frac{\tau}{\tau_\mathrm{d}}}\mathrm{d}\upsilon}{(1+\upsilon^2)^2} \geq \frac{1}{(1+R^2)^2}\int_0^R \mathrm{e}^{-\upsilon^2\frac{\tau}{\tau_\mathrm{d}}}\mathrm{d}\upsilon = \frac{1}{(1+R^2)^2}\sqrt{\frac{\tau_\mathrm{d}}{\tau}}erf(R). \quad (7)$$

Experimental results as well as modeling (Levene et al., 2003) indicate that for small waveguides (30–70 nm), R is <0.15, whereas for larger holes, R rarely exceeds 0.25. The lower bound was found to be a markedly better approximation to numerically integrated values for Eq. 5 as shown in Fig. 4. This yields an approximation that is 97.7% accurate or better for small holes. Since the relative error from one fit to another is on the order of 10%, this approximation proves to be acceptable. The final fitting function is (Fig. 4):

$$G(\tau) = G_0\left[\frac{\pi}{4}\left(\left(1-2\frac{\tau}{\tau_d}\right)e^{\frac{\tau}{\tau_d}}\mathrm{erfc}\left(\sqrt{\frac{\tau}{\tau_D}}\right) - \frac{2}{\sqrt{\pi}}\left(\frac{\tau}{\tau_D}\right)^{1/2}\right) - \sqrt{\frac{\tau_d}{\tau}}\frac{\mathrm{erf}(R)}{(1+R^2)^2}\right], \quad (8)$$

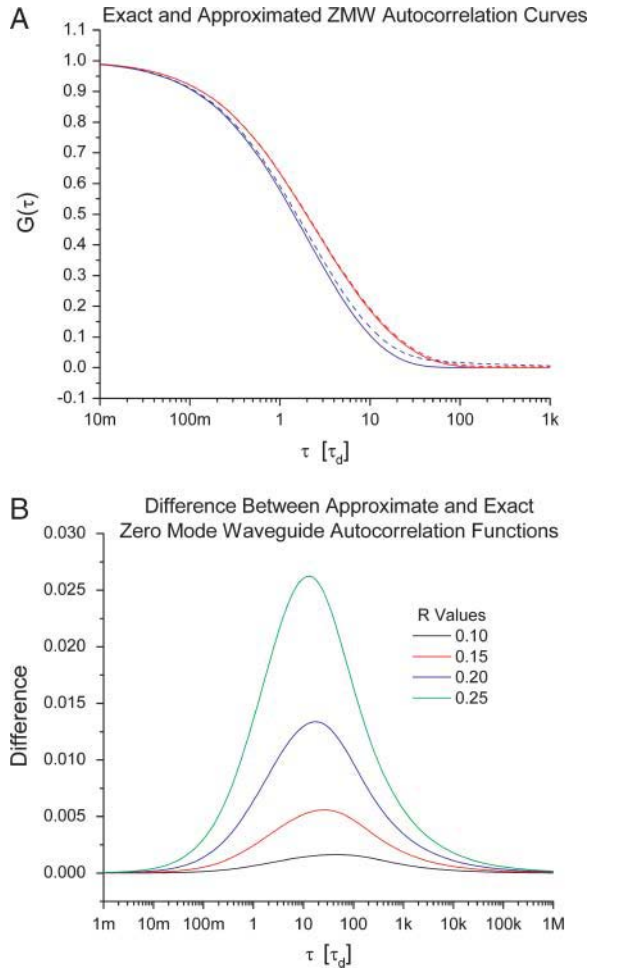

FIGURE 4 (*A*) Plot of the exact (*solid line*) and approximate (*dashed line*) autocorrelation curves for a single diffusing species in a zero-mode waveguide for $R = 0.15$ (*red*) and $R = 0.25$ (*blue*). (*B*) The difference between the approximate and exact autocorrelation curves for $R = 0.10$, 0.15, 0.20, and 0.25. The approximation is quite good for small holes but less reliable for larger ones. The parameters N and τ_d were both set to 1 for these curves.

with free parameters G_0, τ_d, the average residency time in the observation volume, and the geometric ratio R. G_0 is related to the average number of molecules in the focal volume, N, and the constant background signal, B (Koppel, 1974):

$$G(0) = \frac{N}{(N+B)^2}. \quad (9)$$

The factor of $\pi/4$ in Eq. 8 is a normalizing factor required to smoothly combine the one-dimensional diffusion term and the correction term. The one-dimensional diffusion term results from integrating the first integral on the left-hand side of Eq. 5 and is consistent with previous models for one-dimensional diffusion (Starr and Thompson, 2001). A system containing two diffusing species which are statistically independent on the time scale of the experiment can be fit by adding two single species curves together. This yields a total of five free parameters: G_0 and τ_d for each of the species and R, which is defined by the waveguide only.

MATERIALS AND METHODS

Instrumentation

FCS autocorrelation curves were acquired using a confocal fluorescence microscope in epi-illumination mode. Fluorescence was induced using a Melles-Griot Argon-Krypton laser (43 Series; Carlsbad, CA) producing 15 mW at 568 nm. The laser was passed through an excitation filter (Chroma Z568/10X; Chroma, Rockingham, VT), and fluorescence was collected through a dichroic mirror (Chroma Z568RDC; Chroma) and an emission filter (Chroma HQ 630/60M; Chroma). A cover slip corrected 60× water immersion objective with NA 1.2 was used on an Olympus BX51 microscope (Melville, NY). A Newport power meter and beam sampler were used to monitor laser power, and a set of neutral density filters (Chroma) was used to control beam power. A flex02-12D correlator card from correlator.com (Bridgewater, NJ) was used to calculate the FCS autocorrelation curves with a resolution <13 ns, and a PC was then used to acquire and record the intensity trace and autocorrelation function.

Zero-mode waveguides

Zero-mode waveguide arrays were fabricated in a thin but opaque layer of aluminum deposited on a 170 μm fused silica cover slip. Film thicknesses were measured at the time of evaporation by the crystal monitor and again later by a profilometer. Both measurements indicated a film thickness of 100 nm. Electron beam lithography and anisotropic dry etching were used to create a variety of hole sizes. After fabrication, the zero-mode waveguides

TABLE 1 it parameters and results from CI kinetics study

$G^{-1}(0)_{dim}$	1.2 ± 0.3
$G^{-1}(0)_{tet}$	12 ± 4
$\tau_{d,dim}$	$1.6 \times 10^{-5} \pm 3 \times 10^{-6}$
$\tau_{d,tet}$	$2.6 \times 10^{-3} \pm 4 \times 10^{-4}$
R	$.14 \pm 0.03$
V_{obs} (zl)	15 ± 4
K_{D2} (M)	$4.6 \times 10^{-6} \pm 3 \times 10^{-7}$
[CI] (μM)	0.94 μM
N_{dim}	$4 \times 10^{-3} \pm 1 \times 10^{-3}$
N_{tet}	$4.6 \times 10^{-4} \pm 9 \times 10^{-5}$
Background	0.06 ± 0.01

were attached to 12-μL glass wells using UV curable glue and exposed to a low power oxygen plasma to condition the surface. After a sample was placed in a well, it was sealed using a small polydimethylsiloxane slab.

Preparation of CI and O_R1

CI was amplified from λ DNA (New England Biolabs; Beverly, MA; EB N3011S) by polymerase chain reactionand cloned into the BamHI site of expression vector pPROTet.E133 (BD Biosciences Clontech, Palo Alto, CA to yield pPROTet133:CI. Plasmid DNA samples with inserts of the correct size were purified and checked for CI expression by standard immunity tests using superinfection of plasmid-carrying strains with wild-type λ, λvir, and λi^{434} (Arber et al., 1983). mRFP was then fused at the N-terminus of CI by cloning mRFP into pPROTet133:CI using standard methods (Sambrook and Russell, 2001) and checked again for immunity. At this stage the fusion was also checked by DNA sequencing. pPROTet133 is an expression vector in which the cloned gene is fused to a histidine asparagine hexamer (HN_6), and this tag at the N-terminus was used to purify the fusion protein on a cobalt column according to the manufacturer's protocol. The purified protein was then tested for in vitro activity by standard gel shift assays (Sambrook and Russell, 2001) using a 200 basepair λ fragment containing all three right operator sequences labeled at the 5′ end with either ^{32}P or Alexa-fluor 488. The band shift assay exhibited the expected dependence on protein concentration, and binding could be completed by excess unlabeled fragment but not by a random 19-mer of the same base composition. The 17 basepair OR_1 sequence (TATCACCGCCAGAGGTA) and its complement were synthesized by standard methods, annealed, and purified by agarose gel electrophoresis.

Data analysis

The strategy for analyzing FCS curves acquired in the waveguides is to fit the data to Eq. 8 with G_0, R, and τ_d as free parameters. Interestingly, from the definition of τ_d and R, it is easily seen that the value of L need never actually be determined, hence eliminating the need for a precise calibration of the waveguides. Instead it is sufficient to accurately measure the depth of the structures and calculate the diffusion constant from the equation

$$D = \frac{R^2H^2}{\tau_d}, \tag{10}$$

where R and τ_d are empirical parameters and H is well known from the fabrication process. FCS autocorrelation functions are dependant on the diffusion time of the fluorescent species (Elson and Magde, 1974). That diffusion time is in turn dependent on the geometry of the observation volume and the transport properties of the system. Because the parameters that constitute the diffusion time typically do not appear anywhere else in the model autocorrelation function, virtually all FCS techniques require calibration so that transport properties can be derived from the diffusion time. In the case of the zero-mode waveguides, the geometrical parameter describing the observation volume appears in both the diffusion time and the parameter R. Consequently, repeated calibration is replaced by a single, accurate measurement of the waveguide depth.

Autocorrelation curves were fit to the model in Eq. 8 using Matlab's nonlinear curve fitting routines and the Levenberg-Mardquart algorithm. Free parameters were $G_{0,dim}$, $\tau_{d,dim}$, $G_{0,tet}$, $\tau_{d,\ tet}$, and R. The R^2 (residual) values were all >.998, indicating good fits. The values obtained for R agree with theoretical predictions for the waveguides' behavior.

RESULTS AND DISCUSSION

To explore the repressor's oligomerization behavior at high concentrations, an ~1 μM solution of mRFP-CI was prepared and observed in the zero-mode waveguides. At this concentration, dimers and tetramers should be the dominant species, with the tetramers having the larger diffusion constant (Pray et al., 1998). Sets of FCS curves were taken in several waveguides of differing diameter (Fig. 5) and fit using a model assuming two diffusing species. The fit yields $G_{0,dim}$ and $G_{0,tet}$, related to the average number of dimers and average number of tetramers in the observation volume, as well as $\tau_{d\ dim}$ and $\tau_{d\ tet}$, the dimer and tetramer diffusion times, and the geometric ratio R. The values obtained from one waveguide are summarized in Table 1. Equation 10 can be used to calculate the diffusion constants directly from the fit parameters; however, it is illuminating to plot the diffusion times as a function of the geometric factor R. As can be seen in Fig. 6, which shows the diffusion time and R parameters plotted for groups of FCS curves taken from several different waveguides, the data conform reasonably well to the expected quadratic relationship. Interestingly, the variations from curve to curve taken in a single waveguide conform to the same quadratic relationship. This suggests that there are small variations in the illumination profile as a function of time. And it seems likely that small shifts in stage or laser position give rise to these variations. Laser intensity was stable over the time period of the experiment. Despite the clear trend relating the diffusion time to the parameter R, neither $G_{0,dim}$ nor $G_{0,tet}$ displayed any notable dependence on R. This is unexpected, since an increase in diffusion time is assumed to be due to an increase in the total observation volume and a larger observation volume should admit more molecules.

The lack of correlation between G_0 and R was due to a larger problem. Zero-mode waveguides produce a considerable, constant background. A portion of this constant background was likely due to reflection of the excitation illumination. The use of a fiber with a 50-micron core and a 60× objective implies that the photodiode was observing an area ~0.4

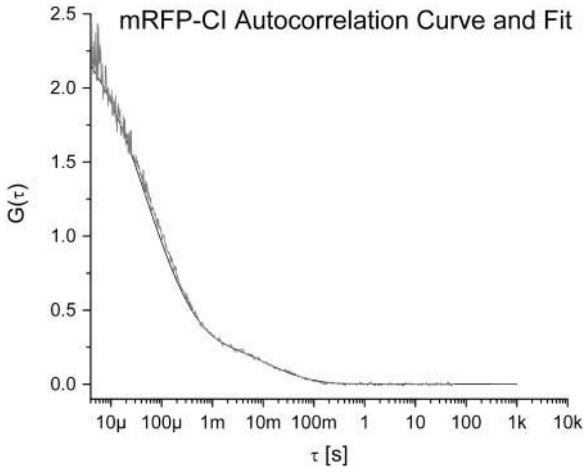

FIGURE 5 Representative autocorrelation curve and fit from the kinetics measurements. Two distinct time constants are visible in the autocorrelation curve. Fit is in black.

TABLE 2 Fit parameters and results from DNA-repressor binding study

Sample	$G^{-1}(0)$	τ_d (s)	R	V_{obs} (zl)	D (cm^2/s)
mRFP-CI	2.7 ± 0.2	$1.4 \times 10^{-5} \pm 2 \times 10^{-6}$	0.17 ± 0.03	25 ± 4	$2.2 \times 10^{-7} \pm 4 \times 10^{-8}$
mRFP-CI/O_R1	49 ± 3	$8.8 \times 10^{-5} \pm 7 \times 10^{-6}$	0.203 ± 0.008	42 ± 1	$4.7 \times 10^{-8} \pm 3 \times 10^{-9}$

microns in radius. Since the waveguides are on the 50 nm scale, and aluminum is an extremely reflective metal, a large fraction of the illumination must be reflected. The use of high quality fluorescence filters produces at least an optical density 6 reduction in the intensity of the excitation line. For traditional fluorescence techniques, this is more than sufficient and yields a good signal-to-noise ratio. When observing single molecules in zero-mode waveguides, however, the relatively weak signal may still be small compared to the transmitted excitation line.

An additional source of background was optical transmission through the waveguides. The objective focuses as much as a milliwatt of laser power on a spot only a few microns across. Consequently, the local optical power density is high enough that the waveguide cannot totally attenuate the excitation line. The resulting weak transmission excited the concentrated solution of fluorophores in the reservoir above the waveguide and, as a result, a constant background was coupled back into the waveguide and detected by the photodiode. This background is proportional to the decay profile through the waveguide squared: once as the excitation passes through the guide and once again as the fluorescence passes back to the detector. In contrast, signal from the observation volume is proportional to the decay profile cubed:

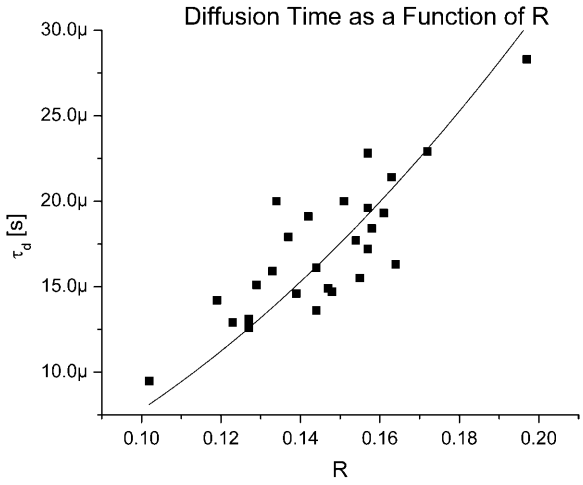

FIGURE 6 A molecule's diffusion time is expected to vary with the size of the zero-mode waveguide being used for the observation. Plotted here are the diffusion time and R parameters for FCS curves taken in several different waveguides. The solid line is a plot of $\tau_d(R) = AR^2$. With $A = 7.6 \times 10^{-4} \pm 2 \times 10^{-5}$ s established by fitting the data. Equation 7 suggests that $A = H^2/D$, implying that $D = 1.3 \times 10^{-7}$ cm^2/s.

once for the excitation profile, once for the coupling interaction, and once for the inhibited emission behavior. As a result, the background should have a considerably weaker dependence on waveguide size than does the signal.

The zero-mode waveguide fabrication procedure included a dry chlorine process to etch the waveguides into the aluminum film. Chlorine is known to etch fused silica, albeit at a rate 10 times slower (Williams and Muller, 1996) than aluminum. This etch is thought to produce small wells at the bottom of the waveguides. Any fluorophore that passes entirely through the waveguide into these subwaveguide glass wells was illuminated uniformly at full excitation intensity and suffers no coupling or radiation attenuation. Consequently, a small glass well beneath the waveguide will produce an intense background signal. Even a few seconds of etching can produce volumes an order of magnitude larger than the waveguide observation volume. Unlike the previous background sources, the fluorescence intensity from the wells should be strongly dependent on the size of the waveguide because the waveguide itself acted as an etch mask.

Though the background has no impact on the measurement of diffusion times, it depresses G_0 from its expected value and must be characterized if meaningful kinetics measurements are to be made. A detailed and comprehensive analysis of the sources and intensities of the background would be a difficult task. However, the data can be background corrected without any specific knowledge of the intensity or source of the constant background signal. The equilibrium constant characterizing the tetramerization of CI should be determined wholly by the ratio N_{tet}/N_{dim}. Consequently, it is important to note that N is not a linear function of B (Eq. 9). If it were, then the background could be disregarded entirely, confident that the effects would cancel out. The correction can be accomplished by solving the following nonlinear system:

$$\begin{aligned} 4N_{tet} + 2N_{dim} &= V_{obs}N_A[CI]_T \\ (G_{0,tet}N_{tet})^{\frac{1}{2}} - G_{0,tet} &= (G_{0,dim}N_{dim})^{\frac{1}{2}} - G_{0,dim}, \end{aligned} \qquad (11)$$

where N_A is Avagadro's Number, $[CI]_T$ is the total concentration of CI monomer, and N denotes the background corrected average number of molecules in the observation volume. The top part of Eq. 11 requires that the total number of diffusing particles conform to the known total concentration of protein monomer.The bottom part of Eq. 11 requires that the background, B, relating G_0 and N, be identical for both the tetramer and dimer. The last condition forces the

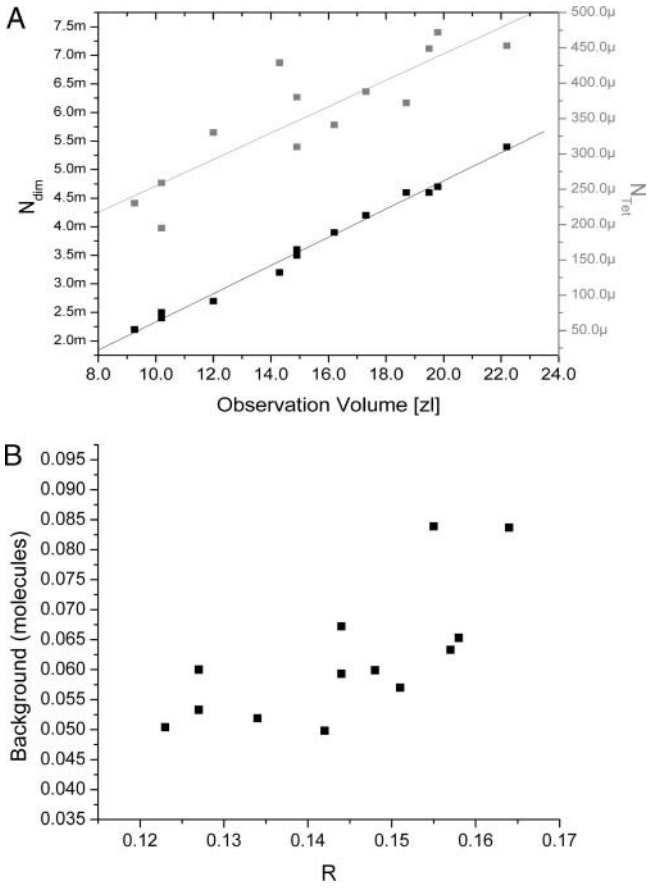

FIGURE 7 Results from background correction. (*A*) Number of dimers and tetramers in the observation volume plotted as a function of the observation volume. Linear fits reveal the concentrations of the two species. $[N_{dim}] = 0.4\ \mu M$. $[N_{tet}] = 0.03\ \mu M$. (*B*) The background, *B*, is seen here to have a dependence on the parameter *R* and, hence, on the size of the waveguide.

background corrected data to conform to the nonlinearity inherent in Eq. 9 while ensuring that only a single background is associated with each autocorrelation curve. The raw and corrected data are summarized in Table 1.

The trends and values of the corrected data are entirely as expected. Whereas the original $G_{0,dim}$ and $G_{0,tet}$ values showed no significant dependence on *R* and hence the observation volume, the corrected data exhibit the expected linear relationship (Fig. 7 *A*). Fitting the data to a line yields the concentration of dimer or tetramer in solution. Additionally, the background, *B*, exhibits a dependence on *R* (Fig. 7 *B*). This is expected since the volume of the subwaveguide well depends on hole size. With the corrected data, the tetramerization constant can be calculated from the definition or a volume independent formula:

$$K_{D2} = \frac{[CI_2]^2}{[CI_4]} = \frac{1}{N_A V_{obs}} \frac{N_{dim}^2}{N_{tet}} = \frac{[CI]_T}{4\left(\frac{N_{tet}}{N_{dim}}\right)^2 + 2\left(\frac{N_{tet}}{N_{dim}}\right)}, \quad (12)$$

where N_A is Avagadro's Number and V_{obs} is the observation volume calculated from Eq. 2. The results from other waveguides were similar, yielding a final value for the tetramerization constant of $K_{D2} = 4.6 \times 10^{-6} \pm 3 \times 10^{-7}$ M. The equilibrium constant is expected to be a function of temperature, which was not precisely controlled in these experiments. Some heating is expected as a result of laser illumination; however, due to the high reflectivity of aluminum, water's low absorption at 568 nm, and temperature regulating effect of the bulk solution, the effect should be small (Lide, 2003). The free energy change associated with tetramerization was measured by Pray, Burz, and Ackers at temperatures between 5°C and 45°C (Pray et al., 1998). The corresponding equilibrium constant, related by the well known equation $\Delta G = -RT\ln K$ was $4 \times 10^{-6} \pm 1 \times 10^{-6}$ M at 20°C, 25°C, and 30°C. The same study indicated that the rate limiting step in CI octamerization is the formation of tetramers (Pray et al., 1998). The free energy change for the tetramer to octamer transition is larger than the change from dimer to tetramer. Consequently, tetramers in solution will quickly become octamers. Although this may introduce some error into the calculated K_{D2} value, the formation of octamers should be limited by the low concentration of tetramers.

With the diffusion constants for the dimer and tetramer firmly established, it was possible to confirm that the repressor proteins retained their ligand binding activity. CI has evolved to strongly and specifically bind to the O_R1 operator site (Ptashne, 1992). To assay that the mRFP-CI bound the O_R1 sequence, fluorescence autocorrelation curves were obtained from mRFP-CI with O_R1 in solution. The experiments were constrained by the need to have the concentration of O_R1 DNA fragments exceed the total concentration of CI dimers and CI tetramers in solution. With the K_{D2} value determined, the appropriate total mRFP-CI concentration could be chosen and data could be acquired in zero-mode waveguide suitable for use at concentrations of $\sim 1\ \mu M$. Solutions containing 1 μM mRFP-CI, 2.4 uM O_R1 and diluted in the standard Sauer binding buffer were prepared, and a series of 10 autocorrelation curves were acquired (Johnson et al., 1980; Fig. 8). Because the ratio of operator sequence to repressor oligomer was more than 2:1 and k_b for the operator binding on the order of 10^{-9}, all the fluorescent repressor multimers are expected to have bound a DNA fragment. The results are summarized in Table 2. When in the presence of the O_R1 DNA fragment, the dimeric mRFP-CI exhibited a diffusion constant more than 4 times smaller than without the operator sequence. Although the DNA fragment is relatively small, it causes a significant reduction of the diffusion constant which may be due to the highly charged DNA backbone. Unfortunately, it is difficult to compare diffusion constants with previous studies because changes in size, total charge, or buffer concentrations can significantly alter the transport properties of an analyte in solution.

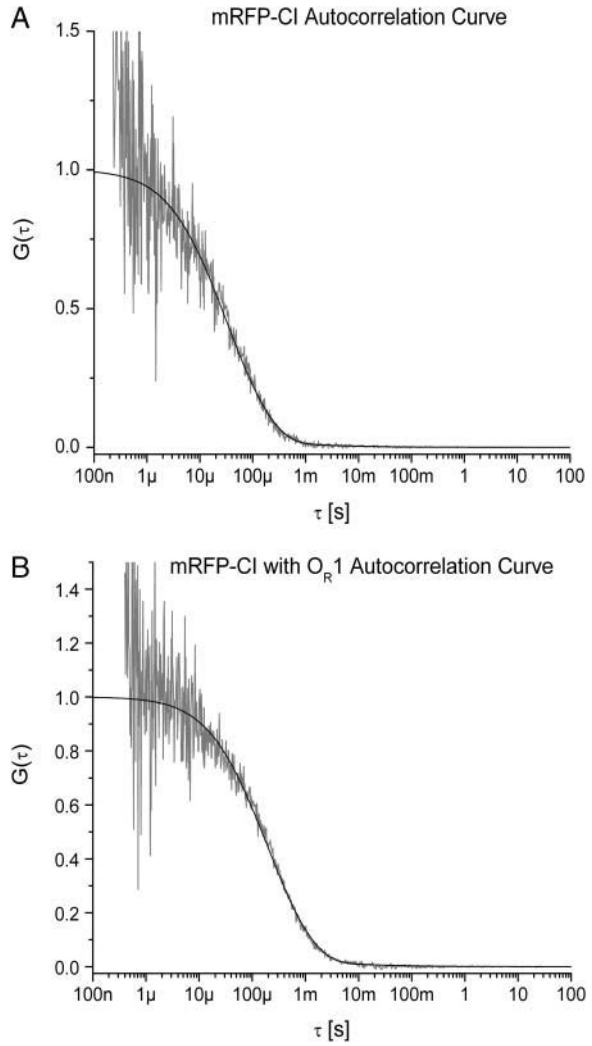

FIGURE 8 Representative autocorrelation curves from (*A*) the mRFP-CI sample and (*B*) the O_R1 with mRFP-CI sample. The full width at half-maximum provides a good estimate of the diffusion time. Because the curves were acquired in two waveguides of differing size and observation volume, the diffusion times cannot simply be compared. Instead, the diffusion constants must be calculated. Both curves have G_0 normalized to 1. Fits are in black.

CONCLUSION

We have shown here that FCS in zero-mode waveguides is an effective technique for studying biosystems at high concentrations. The above results demonstrate that for oligimerization reactions, total concentrations in the micromolar range are accessible. Because waveguide fabrication is fast and simple, devices can be tailor made to work at a wide range of concentrations without significantly altering the data acquisition or analysis procedures. The virtues of the technique include the use of fluorescent probes, which are abundant, and labeling procedures, which are typically simple. The subwavelength dimensions of the waveguides and the ability to fabricate large arrays make them ideal for massively parallel data acquisition as well as sensitive single molecule studies. Since various fluorescence-based assays can be done in the waveguides, they are a perfect tool for fields such as drug development, where the effects of many compounds on a target system must be characterized.

The authors thank Dr. Warren Zipfel for helpful conversation and Fig. 2.

This work was supported by the Department of Eergy, by the Defense Advanced Research Projects Agency, and by the National Institutes of Health (NIH HG001506). Fabrication was done at the Cornell Nano-Scale Science and Technology Facility supported by National Science Foundation grant ECS-9731293, its users, Cornell University, and industrial partners.

REFERENCES

Arber, W., L. Enquist, B. Hohn, N. E. Murray, and K. Murray. 1983. Experimental methods for use with lambda. *In* LAMBDA II. R. W. Hendrix, J. W. Roberts, F. W. Stahl, and R. A. Weisberg, editors. Cold Spring Harbor Laboratory Press, Cold Spring Harbor, NY. 433–466.

Betzig, E., and R. J. Chichester. 1993. Single molecules observed by near-field scanning optical microscopy. *Science*. 262:1422–1425.

Burz, D. S., and G. K. Ackers. 1996. Cooperativity mutants of bacteriophage lambda cI repressor: temperature dependence of self-assembly. *Biochemistry*. 35:3341–3350.

Cluzel, P., M. Surette, and S. Leibler. 2000. An ultrasensitive bacterial motor revealed by monitoring signaling proteins in single cells. *Science*. 287:1652–1655.

de Lange, F., A. Cambi, R. Huijbens, B. de Bakker, W. Rensen, M. Garcia-Parajo, N. van Hulst, and C. G. Figdor. 2001. Cell biology beyond the diffraction limit: near-field scanning optical microscopy. *J. Cell Sci*. 114: 4153–4160.

Dodd, I. B., A. J. Perkins, D. Tsemitsidis, and J. B. Egan. 2001. Octamerization of lambda CI repressor is needed for effective repression of P-RM and efficient switching from lysogeny. *Genes Dev*. 15:3013–3022.

Elson, E. L., and D. Magde. 1974. Fluorescence correlation spectroscopy. 1. Conceptual basis and theory. *Biopolymers*. 13:1–27.

Foquet, M., J. Korlach, W. R. Zipfel, W. W. Webb, and H. G. Craighead. 2004. Focal volume confinement by submicrometer-sized fluidic channels. *Anal. Chem*. 76:1618–1626.

Gennerich, A., and D. Schild. 2000. Fluorescence correlation spectroscopy in small cytosolic compartments depends critically on the diffusion model used. *Biophys. J*. 79:3294–3306.

Hess, S. T., and W. W. Webb. 2002. Focal volume optics and experimental artifacts in confocal fluorescence correlation spectroscopy. *Biophys. J*. 83:2300–2317.

Jackson, J. D. 1999. Classical Electrodynamics. Wiley & Sons, New York.

Johnson, A. D., C. O. Pabo, and R. T. Sauer. 1980. Bacteriophage lambda repressor and cro protein: interactions with operator DNA. *Methods Enzymol*. 65:839–856.

Koppel, D. E. 1974. Statistical accuracy in fluorescence correlation spectroscopy. *Phys. Rev. A*. 10:1938–1945.

Levene, M. J., J. Korlach, S. W. Turner, M. Foquet, H. G. Craighead, and W. W. Webb. 2003. Zero-mode waveguides for single-molecule analysis at high concentrations. *Science*. 299:682–686.

Lide, D. R. 2003. CRC Handbook of Chemistry and Physics, 84th ed. CRC Press, Boca Raton, FL.

Mashanov, G. I., D. Tacon, A. E. Knight, M. Peckham, and J. E. Molloy. 2003. Visualizing single molecules inside living cells using total internal reflection fluorescence microscopy. *Methods*. 29:142–152.

McCain, K. S., P. Schluesche, and J. M. Harris. 2004. Modifying the adsorption behavior of polyamidoamine dendrimers at silica surfaces investigated by total internal reflection fluorescence correlation spectroscopy. *Anal. Chem.* 76:930–938.

Pray, T. R., D. S. Burz, and G. K. Ackers. 1998. Cooperative non-specific DNA binding by octamerizing lambda cI repressors: a site-specific thermodynamic analysis. *J. Mol. Biol.* 282:947–958.

Ptashne, M. 1992. A Genetic Switch. Cell Press and Blackwell Science, Cambridge, MA.

Rischel, C., L. E. Jorgensen, and Z. Foldes-Papp. 2003. Microsecond structural fluctuations in denatured cytochrome c and the mechanism of rapid chain contraction. *J. Phys. Condens. Matter.* 15:S1725–S1735.

Sambrook, J., and D. W. Russell. 2001. Molecular Cloning. Cold Spring Harbor Press, Cold Spring Harbor, NY.

Schmiedeberg, L., K. Weisshart, S. Diekmann, G. M. Z. Hoerste, and P. Hemmerich. 2004. High- and low-mobility populations of HP1 in heterochromatin of mammalian cells. *Mol. Biol. Cell.* 15:2819–2833.

Starr, T. E., and N. L. Thompson. 2001. Total internal reflection with fluorescence correlation spectroscopy: combined surface reaction and solution diffusion. *Biophys. J.* 80:1575–1584.

Webb, W. W. 2001. Fluorescence correlation spectroscopy: inception, biophysical experimentations, and prospectus. *Appl. Opt.* 40:3969–3983.

Williams, K. R., and R. S. Muller. 1996. Etch rates for micromachining processing. *J. Microelectromech. Syst.* 5:256–269.